Simultaneous P-P and P-S inversion by weighted stacking applied to the Blackfoot 3C-3D survey

Jeffrey A. Larsen, Gary F. Margrave, Han-xing Lu and Colin C. Potter

ABSTRACT

A joint P-P and P-S weighted stacking method has been implemented to extract elastic parameters from multi-component seismic data. This method uses separately processed P-P and P-S data volumes, each consisting of a series of migrated limited-offset data volumes. These offset data volumes for the P-P and P-S datasets (each representing an offset range at the target of interest) are then weighted and summed to form two separate data volumes representing fractional P-wave and shear velocity estimates. These data volumes can thus be used to correlate anomalous P-wave and shear velocities that can thus be related to lithology and pore fluid content changes. This method is compared to a stand-alone P-wave weighted stacking method using the reprocessed Blackfoot 3C-3D data. Initial results show that the inclusion of P-S data gives similar or better results than standard P-wave methods alone.

INTRODUCTION

AVO analysis and inversion techniques have been used throughout the world in a variety of situations with varied rates of success. Among the most successful methods to date has been the weighted stacking technique first proposed by Smith and Gidlow (1987), that provides a quick and robust method for AVO analysis. This method can be used in a standard seismic data processing sequence to display information about rock matrix and pore fluid properties in the form of a stacked section. It also provides estimates of fractional changes in P-wave and shear velocities that are thus related to rock properties (Castagna, 1993). One problem inherent with the Smith and Gidlow approach was the incorporation of Gardner's relation, which may or may not be applicable in a given lithology. This method was further developed by Fatti et al. (1994) to eliminate this dependency upon Gardner's relation to estimate density. Recent work has shown that improved lithology and pore fluid prediction can be obtained using Lame's parameters (Goodway et al., 1997).

A number of authors have demonstrated the utility of combined AVO analysis using P-P, P-S and S-S modes (Garotta and Granger, 1987, Miles and Gassaway, 1989). In an effort to constrain some of the problems inherent in standard weighted stacking schemes, Stewart (1990) developed a joint P-P and P-S weighted stacking technique. This method while maintaining the robustness of the P-wave weighted stacking technique has the benefit of data redundancy provided by the converted wave data. Since changes in R_{pp} are partially controlled by the conversion of P-wave energy into S-wave energy, R_{pp} has a partial dependence on the shear velocity. By contrast, converted wave (P-S) reflectivity is generally more dependant on S-wave velocities (Danbom and Domenico, 1986). This effect can be easily seen in the Aki and Richards (1980) Zoeppritz equation approximations.

Contents

The Smith and Gidlow method, or the "Geostack method" uses an empirical relationship between V_P and V_S. By utilizing the additional measurement of the converted reflectivity R_{PS}, these parameters can be estimated without the need for an empirical relationship between V_P and V_S. Given careful processing and correlation of the converted wave dataset, this joint P-P and P-S weighted stacking method should provide better estimates of elastic parameters compared with the standard P-wave technique alone.

This paper will first outline a method using both P-P and P-S seismic data to construct weighted stacks. Next, this paper will deal with seismic processing and event correlation concerns using P-P and P-S seismic data. Finally, this method will be applied to the Blackfoot 3C-3D and compared to the Smith & Gidlow method.

THEORY

Smith and Gidlow Method

The Zoeppritz equations fully describe the relationship between incident, reflected and transmitted P and S plane waves on either side of a plane interface. These equations are both complex to use and difficult to solve. It was therefore deemed necessary to create a more robust approximation to the Zoeppritz equations. Koefoed (1955), Aki and Richards (1980) and Shuey (1985) have developed approximations for P-P reflection coefficients. The equation used here is the Aki and Richards approximation for P-P reflectivity

$$R_{PP}(\theta) \approx \frac{1}{2}\left(1 - 4\frac{\beta^2}{\alpha^2}\sin^2\theta\right)\frac{\Delta\rho}{\rho} + \frac{1}{2\cos^2\theta}\frac{\Delta\alpha}{\alpha} - \frac{4\beta^2}{\alpha^2}\sin^2\theta\frac{\Delta\beta}{\beta} \qquad (1)$$

where α, β, ρ are the average P-wave, S-wave and density values across an interface, $\Delta\alpha$, $\Delta\beta$, $\Delta\rho$ are the P-wave, S-wave and density contrasts across an interface, and θ is the average of the P-wave angle of incidence and transmission across the interface.

Equation (1) assumes small relative changes in α, β and ρ across an interface which allows higher order terms to be neglected. Also, θ must also not approach a critical angle or ninety degrees in this approximation.

Following the application of Gardner's relation (Gardner et al., 1974) relating compressional velocity and density, Smith and Gidlow show that equation (1) can be written as

$$R_{PP}(\theta) \approx A(\theta)\frac{\Delta\alpha}{\alpha} + B(\theta)\frac{\Delta\beta}{\beta} \qquad (2)$$

In a v(z) medium, the angle dependant weights $A(\theta)$ and $B(\theta)$, can easily be directly related to offset with simple raytracing. This raytracing procedure as well as α and β estimates can be obtained using a velocity-depth model obtained from well logs in the area of interest. These offset dependant weights are given by

Contents

$$A(\theta) = \frac{5}{8} - \frac{1}{2}\frac{\beta^2}{\alpha^2}\sin^2\theta + \frac{1}{2}\tan^2\theta \tag{3}$$

$$B(\theta) = -4\frac{\beta^2}{\alpha^2}\sin^2\theta \tag{4}$$

where θ is calculated for each time sample in a given NMO corrected CMP gather.

Equation (2) is now sufficiently robust to apply a least-squares inversion procedure to obtain values for $\Delta\alpha/\alpha$ and $\Delta\beta/\beta$. The solution to this least-squares inversion has the form:

$$\frac{\Delta\alpha}{\alpha} = \sum_{i=1}^{N}\left[Rpp_i \frac{A_i\sum_{j=1}^{N}\left(B_j^2\right) - B_i\sum_{j=1}^{N}\left(A_jB_j\right)}{\sum_{j=1}^{N}\left(A_j^2\right)\sum_{j=1}^{N}\left(B_j^2\right) - \left(\sum_{j=1}^{N}A_jB_j\right)^2}\right], \tag{5}$$

$$\frac{\Delta\beta}{\beta} = \sum_{i=1}^{N}\left[Rpp_i \frac{B_i\sum_{j=1}^{N}\left(A_j^2\right) - A_i\sum_{j=1}^{N}\left(A_jB_j\right)}{\sum_{j=1}^{N}\left(A_j^2\right)\sum_{j=1}^{N}\left(B_j^2\right) - \left(\sum_{j=1}^{N}A_jB_j\right)^2}\right]. \tag{6}$$

In these expressions R_{PPi} represents P-wave seismic data at a discrete offset and the summation is taken over all offsets. Equations (3) and (4) can thus provide estimates of $\Delta\alpha/\alpha$ and $\Delta\beta/\beta$ using properly processed pre-stack NMO corrected seismic data. A number of procedures and assumptions must first be included in the processing of this seismic data

1. The source signature must be first removed via an appropriate deconvolution.

2. The data must be relatively free of noise, multiple events and mode conversions, several procedures are recommended:

   - linear noise removal using f-k filtering

   - parabolic radon filtering for multiple attenuation

   - common offset or limited-offset stacking for random noise attenuation

3. Correct reflection coefficient amplitudes must be maintained, trace equalization and statistical methods of amplitude recovery such as AGC must be avoided.

4. Appropriate steps should be undertaken to increase the bandwidth of the seismic data without significantly increasing random noise.

Contents

5. Careful statics and NMO procedures are necessary. It is recommended that NMO be followed by residual NMO (RNMO).

6. Pre-stack migration / DMO should be used to increase lateral resolution to better than the Fresnel zone width. An amplitude preserving algorithm should be used in this process.

Smith and Gidlow further formed equations (5) and (6) into two factors: the pseudo-Poisson's ratio reflectivity and the fluid factor reflectivity.

$$\frac{\Delta\sigma}{\sigma} = \frac{\Delta\alpha}{\alpha} - \frac{\Delta\beta}{\beta} \tag{7}$$

$$\Delta f = \frac{\Delta\alpha}{\alpha} - 1.16\frac{\beta}{\alpha}\frac{\Delta\beta}{\beta} \tag{8}$$

The pseudo-Poisson's ratio can also be thought of as a fractional change in the ratio of V_P/V_S:

$$\frac{\Delta(\alpha/\beta)}{\alpha/\beta} = \frac{\beta}{\alpha}\left[d\left(\frac{\alpha}{\beta}\right)\right] = \frac{\beta}{\alpha}\left(\frac{1}{\beta}d\alpha - \frac{\alpha}{\beta^2}d\beta\right) = \frac{\Delta\alpha}{\alpha} - \frac{\Delta\beta}{\beta} \tag{9}$$

The fractional velocity estimates ($\Delta\alpha/\alpha$, $\Delta\beta/\beta$) and the pseudo-Poisson's ratio reflectivity are general indicators of lithology and pore-fluid content (Swan, 1993). The fluid factor reflectivity, by contrast, is designed as a specific indicator of gas-saturated clastic sedimentary rocks. This factor is designed to be low amplitude for all reflectors in a clastic sedimentary sequence except rocks that lie off the mudrock line (Fatti et al., 1994). Rocks that lie off the mudrock line include gas-saturated clastics, carbonates and igneous rocks.

Stewart's joint P-P and P-S weighted stacking method

This method is developed in much the same way as the Smith and Gidlow method except for the inclusion of P-S reflectivities. Equations (10) and (11) are from the Aki and Richards approximations for P-P and P-S reflectivities respectively:

$$R_{PP}(\theta) \approx \frac{1}{2}\left(1 - 4\frac{\beta^2}{\alpha^2}\sin^2\theta\right)\frac{\Delta\rho}{\rho} + \frac{1}{2\cos^2\theta}\frac{\Delta\alpha}{\alpha} - \frac{4\beta^2}{\alpha^2}\sin^2\theta\frac{\Delta\beta}{\beta} \tag{10}$$

$$R_{PS}(\theta) \approx \frac{-\alpha\tan\varphi}{2\beta}\left[\left(1 - \frac{2\beta^2}{\alpha^2}\sin^2\theta + \frac{2\beta}{\alpha}\cos\theta\cos\varphi\right)\frac{\Delta\rho}{\rho} - \left(\frac{4\beta^2}{\alpha^2}\sin^2\theta - \frac{4\beta}{\alpha}\cos\theta\cos\varphi\right)\frac{\Delta\beta}{\beta}\right] \tag{11}$$

where α, β, ρ are the average P-wave, S-wave and density values across an interface, $\Delta\alpha$, $\Delta\beta$, $\Delta\rho$ are the P-wave, S-wave and density contrasts across an interface, θ is the average of the P-wave angle of incidence and transmission across the interface, and φ

Contents

is the average of the converted wave angle of reflection and transmission across the interface.

The application of Gardner's relation between P-wave velocity and density to equations (10) and (11) above (see Stewart, 1990 for details), gives equations of the form

$$R_{PP}(\theta) \approx a(\theta)\frac{\Delta\alpha}{\alpha} + b(\theta)\frac{\Delta\beta}{\beta} \tag{12}$$

$$R_{PS}(\theta) = c(\theta)\frac{\Delta\alpha}{\alpha} + d(\theta)\frac{\Delta\beta}{\beta} \tag{13}$$

where:

$$a(\theta) = \frac{1}{8}\left(1 - \frac{4\beta^2}{\alpha^2}\sin^2\theta + \frac{4}{\cos^2\theta}\right) \tag{14}$$

$$b(\theta) = -\frac{4\beta^2}{\alpha^2}\sin^2\theta \tag{15}$$

$$c(\theta) = -\frac{\alpha\tan\varphi}{8\beta}\left(1 - \frac{2\beta^2}{\alpha^2}\sin^2\theta + \frac{2\beta}{\alpha}\cos\theta\cos\varphi\right) \tag{16}$$

$$d(\theta) = \frac{\alpha\tan\varphi}{2\beta}\left(\frac{4\beta^2}{\alpha^2}\sin^2\theta - \frac{4\beta}{\alpha}\cos\theta\cos\varphi\right) \tag{17}$$

Equations (12) and (13) can be solved for $\Delta\alpha/\alpha$ and $\Delta\beta/\beta$ by applying a least-squares inversion procedure which results in:

$$\frac{\Delta\alpha}{\alpha} = \frac{\sum(d^2 - b^2)\sum(aR_{PP} - cR_{PS}) - \sum(cd - ab)\sum(bR_{PP} - dR_{PS})}{\sum(c^2 - a^2)\sum(d^2 - b^2) - \left[\sum(cd - ab)\right]^2} \tag{18}$$

$$\frac{\Delta\beta}{\beta} = \frac{\sum(c^2 - a^2)\sum(bR_{PP} - dR_{PS}) - \sum(cd - ab)\sum(aR_{PP} - cR_{PS})}{\sum(c^2 - a^2)\sum(d^2 - b^2) - \left[\sum(cd - ab)\right]^2} \tag{19}$$

where the reflection coefficients R_{PP} and R_{PS} represent P-wave and P-S wave processed seismic data. These reflection coefficients and the weights a, b, c and d are summed over all offsets in a given CMP gather. Equations (18) and (19) can be rearranged to obtain equations directly in terms of weights for both the P-P and P-S reflectivities.

Contents

$$\frac{\Delta\alpha}{\alpha} = \sum_i \left[R_{PP\,i} \frac{a_i \sum_j (d_j^2 - b_j^2) - b_i \sum_j (c_j d_j - a_j b_j)}{\sum_j (c_j^2 - a_j^2) \sum_j (d_j^2 - b_j^2) - \left[\sum_j (c_j d_j - a_j b_j) \right]^2} \right. \tag{20}$$

$$\left. R_{PS\,i} \frac{c_i \sum_j (d_j^2 - b_j^2) - d_i \sum_j (c_j d_j - a_j b_j)}{\sum_j (c_j^2 - a_j^2) \sum_j (d_j^2 - b_j^2) - \left[\sum_j (c_j d_j - a_j b_j) \right]^2} \right]$$

$$\frac{\Delta\beta}{\beta} = \sum_i \left[R_{PP\,i} \frac{b_i \sum_j (c_j^2 - a_j^2) - a_i \sum_j (c_j d_j - a_j b_j)}{\sum_j (c_j^2 - a_j^2) \sum_j (d_j^2 - b_j^2) - \left[\sum_j (c_j d_j - a_j b_j) \right]^2} \right. \tag{21}$$

$$\left. + R_{PS\,i} \frac{c_i \sum_j (c_j d_j - a_j b_j) - d_i \sum_j (c_j^2 - a_j^2)}{\sum_j (c_j^2 - a_j^2) \sum_j (d_j^2 - b_j^2) - \left[\sum_j (c_j d_j - a_j b_j) \right]^2} \right]$$

Again, similar assumptions must be made regarding the processing of the P-P dataset as described previously. The additional complication of the P-S data must be accounted for in several ways. First, since AVO behavior in the P-S mode is generally more variable than the P-P mode (see figure 1), careful amplitude preservation must be maintained or in the case of trace equalized data, the average AVO behavior must be carefully restored.

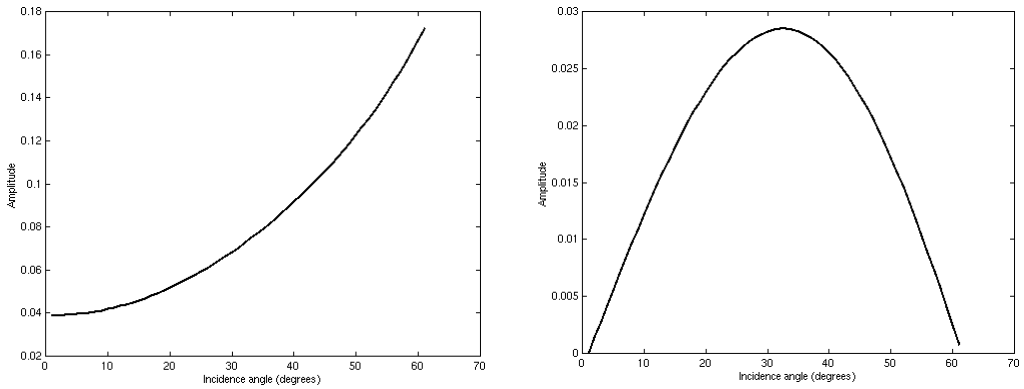

Figure 1: Rpp (left) and Rps (right) curves showing expected AVO behavior for a typical lithological situation using the Zoeppritz equations. Notice the P-S AVO curve exhibits a stronger relative change in reflection coefficient amplitude with offset compared to the P-P curve.

Contents

A processing sequence that equalizes trace amplitudes over offset must be treated with caution. In the case of this study, a procedure has been used to restore the average theoretical behavior of amplitudes in both the P-P and P-S datasets. The following formulas have been applied to correct these datasets.

$$R_{PP}(t,h) = \frac{\int_0^{T_{\max}} \left| S_{\mathrm{mod}\,el\,PP}(t',h) \right| dt'}{\int_0^{T_{\max}} \left| S_{data\,PP}(t',h) \right| dt'} S_{data\,PP}(t,h) \tag{22}$$

$$R_{PS}(t,h) = \frac{\int_0^{T_{\max}} \left| S_{\mathrm{mod}\,el\,PS}(t',h) \right| dt'}{\int_0^{T_{\max}} \left| S_{data\,PS}(t',h) \right| dt'} S_{data\,PS}(t,h) \tag{23}$$

where $R_{PP}(t,h)$ and $R_{PS}(t,h)$ are the corrected reflection coefficient amplitudes at a given time (t) and offset (h), $S_{dataPP}(t,h)$ and $S_{dataPS}(t,h)$ are the reflection coefficient inputs from a trace equalized time sample, and $S_{modelPP}(t,h)$ and $S_{modelPS}(t,h)$ are calculated model-based reflection coefficient amplitudes from an elastic synthetic seismogram. This elastic synthetic seismogram, the SYNTH algorithm (Margrave and Foltinek, 1995) calculates reflection coefficients using the Zoeppritz equations over a range of offset values. This procedure will weight each time sample by its expected model behavior in order to properly preserve its relative amplitude with offset.

Second, radial channel datasets generally include large source and receiver statics. In the case of this study, residual receiver static corrections as large as 150ms were used. The method chosen for these residual receiver statics correction was a common receiver stack, which is valid in areas of relatively horizontal bedding (Lu and Margrave, 1998).

Similarly to the Smith and Gidlow method, equations (20) and (21) can be formed into pseudo-Poisson's ratio reflectivity and fluid factor reflectivity stacks for final display and analysis.

This joint inversion method has been shown to be accurate using synthetic noise-free data (Vestrum and Stewart, 1993). The model chosen in this synthetic study included incident angles as high as 55° for P-P waves and 65° for P-S waves. The model also incorporated substantial changes in α and β beyond the assumptions of small changes in elastic parameters made in the Aki and Richards approximations for P-P and P-S reflectivities. This method should therefore provide a robust method of estimating elastic parameters using multi-component seismic data.

CALCULATION OF WEIGHTS

The calculation of weights for the Smith & Gidlow method and the Stewart simultaneous inversion method are quite similar. First, well logs containing p-wave and s-wave sonic logs are obtained and converted to velocity logs. These velocity logs are then smoothed by fitting a high order polynomial to the velocity curves in a least-squares sense. Incidence angles for P-P and P-S reflections are calculated via

raytracing to each depth level in the dataset of interest using smoothed α and β velocities obtained previously.

EVENT CORRELATION OF P-P AND P-S DATA

The joint inversion outlined in this paper relies upon accurate correlation between P-P and P-S events. A constant assumption for α/β commonly used in converted wave exploration is not sufficient as the value of α/β varies due to lithology and pore fluid content. It was therefore decided in this research to correlate events on the P-P (vertical) and P-S (inline-horizontal) channels directly using time-depth curves. Events were first flattened on the Glauconitic zone (lower Mannville) marker, a regional marker just below the Upper Mannville coals. Velocities for these time-depth curves were obtained from the smoothed velocity logs obtained previously. A small depth interval was selected in this study from the lower Mannville marker to below the Mississippian unconformity (Shunda formation). The lower Mannville pick (in depth) was then made on both the P-P and P-S time-depth curves. Identical events on the P-P and P-S curves can thus be correlated in time relative to the lower Mannville pick. Future work will include a conversion to depth for events on both the P-P and P-S time sections.

PROCESSING OF THE BLACKFOOT 3C-3D

Reprocessing of the Blackfoot 3C-3D survey was completed in late 1998 (Lu and Margrave, 1998). A detailed processing flow for both the vertical and radial channels is also given in the same paper. For analysis of the Blackfoot 3C-3D, a number of limited-offset migrated data volumes were formed for both the P-P and the P-S datasets. Each limited-offset data volume represents an offset range at the zone of interest (Glauconitic channel). For the purposes of this study, a single pass 3D phase-shift migration was used following stacking of each offset range. The offset ranges are summarized in table 1 below:

vertical channel offset range (m)	radial channel offset range (m)	naming convention
0-450	0-700	near
225-675	350-1050	mid-near
450-900	700-1400	mid
675-1135	1050-1750	mid-far
900-1350	1400-2100	far

Table 1: Offset ranges for each dataset and corresponding naming convention

The reflectivity scaling factors in equations (22) and (23) are then applied to the input trace equalized datasets (P-P and P-S). Next, weights are calculated for a subset of values in each offset range, and the average of these values is taken for each offset range. Following the calculation of weights and the correlation of P-P and P-S events for each offset gather, each average weight is multiplied by its appropriate offset range and summed to form estimates of $\Delta\alpha/\alpha$ and $\Delta\beta/\beta$.

EXPECTED RESULTS FROM THE BLACKFOOT FIELD

A detailed description of the geology in the Blackfoot field is described by (Miller et al., 1995). The zone of most interest in this region are the incised valley-fill sediments of the Glauconitic sandstone formation. This formation lies within the Mannville Group of Cretaceous age. The incised valley fill cuts to varying depths through any or all of the underlying clastic strata of the Ostracod, Bantry shale, Sunburst or Detrital formations. This incised valley may cut even further down into carbonates just below the Mississippian unconformity surface (Shunda formation). The Glaucontic member can further be subdivided into three units: the upper and lower porous quartz sandstones, and the non-porous middle-lithic sandstone. Each of these subdivisions of the Glauconitic sandstone can range in thickness from 0–20m. Hydrocarbon accumulations may occur in both the upper and lower members, with gas dominating in the upper, and oil dominating in the lower channel. These lithology variations are represented by well logs shown in figures 2 to 4 (Simin et al., 1996). These well logs were selected because they represent the area as a whole and all contain P-wave sonic, S-wave sonic and density curves. These curves were blocked (averaged over each formation interval) to represent bulk elastic properties in each formation.

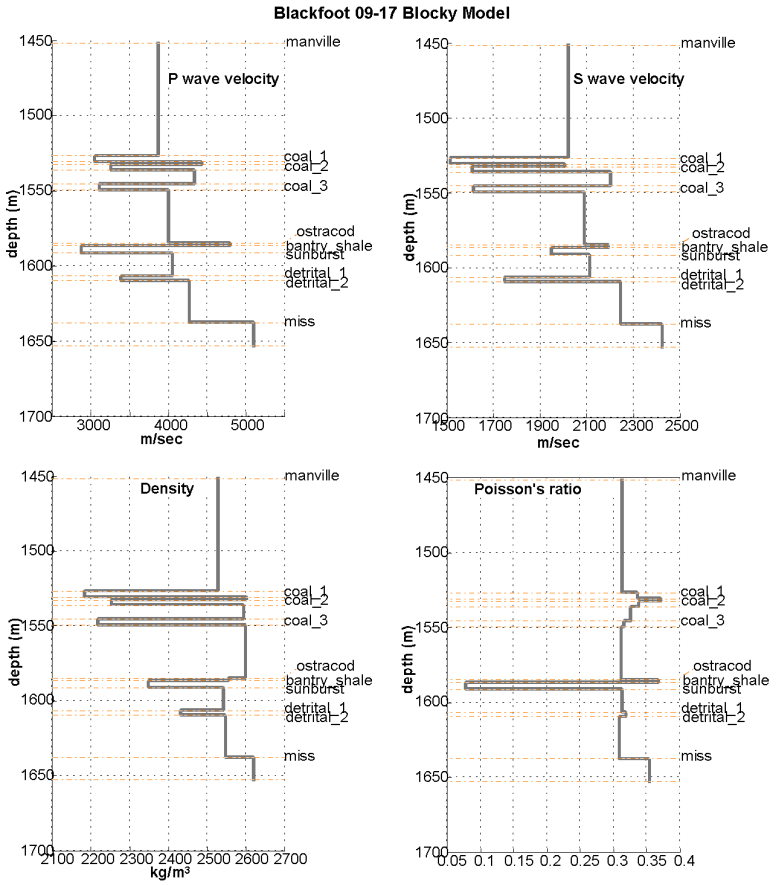

Figure 2: Blocked p-wave, s-wave, density and Poisson's ratio logs for the 09-17 well (regional well) in the Manville to Mississippian interval (after Simin et al., 1996). The strong Poisson's ratio drop at the Bantry shale is believed to be a false effect.

Contents

Well 09-17 (figure 2) is a regional well and represents a zone with no Glauconitic channel deposition. Well 08-08 (figure 3) represents an oil-producing well within the channel zone, here the glauc_ch_top marker is the upper channel, the glauc_1 marker is the middle lithic channel, and the glauc_ss is the top of the lower channel. Notice the significant drop in P-wave velocity and increase in shear velocity at the top of the upper glauconitic, resulting in a significant drop in Poisson's ratio. Well 12-16 (figure 4) also represents a lithology within the channel zone believed to be primarily shale filled, shows a slight drop in Poisson's ratio in the upper channel.

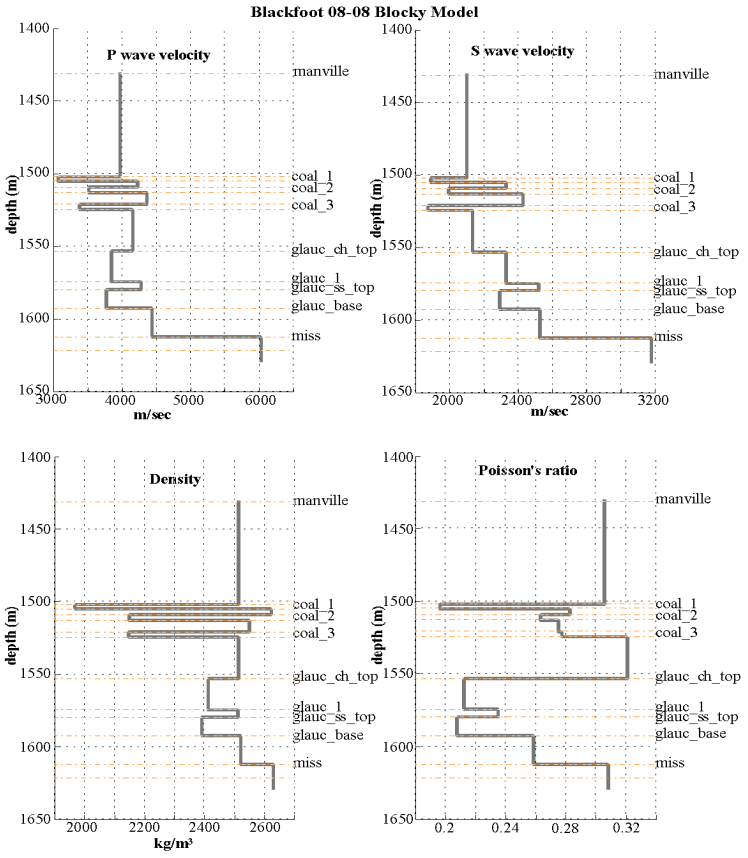

Figure 3: Blocked p-wave, s-wave, density and Poisson's ratio logs for the 8-8 well (after Simin et al., 1996). Notice the strong Poisson's ratio drop (Vp/Vs decrease) at the top of the upper glauconitic channel (glauc_ch_top marker) due to presence of reservoir gas. A much smaller Poisson's ratio decrease can also be observed at the top of the lower channel (glauc_ss_base).

A number of predictions can be made about the P-P and P-S AVO responses in the area of study. Figure 5 below shows plots of reflection coefficient amplitude vs. incidence angle and offset (calculated via ray tracing for P-P and P-S reflections). A strong P-wave AVO anomaly can be seen at the top channel interval due to the large decrease in Poisson's ratio. The P-S reflectivity can be seen to flip polarity from negative (near offset) to positive (far offset). A very weak P-wave AVO anomaly exists at the lower channel top. However, a much stronger P-S AVO anomaly exists at this depth which may be of significance in this study.

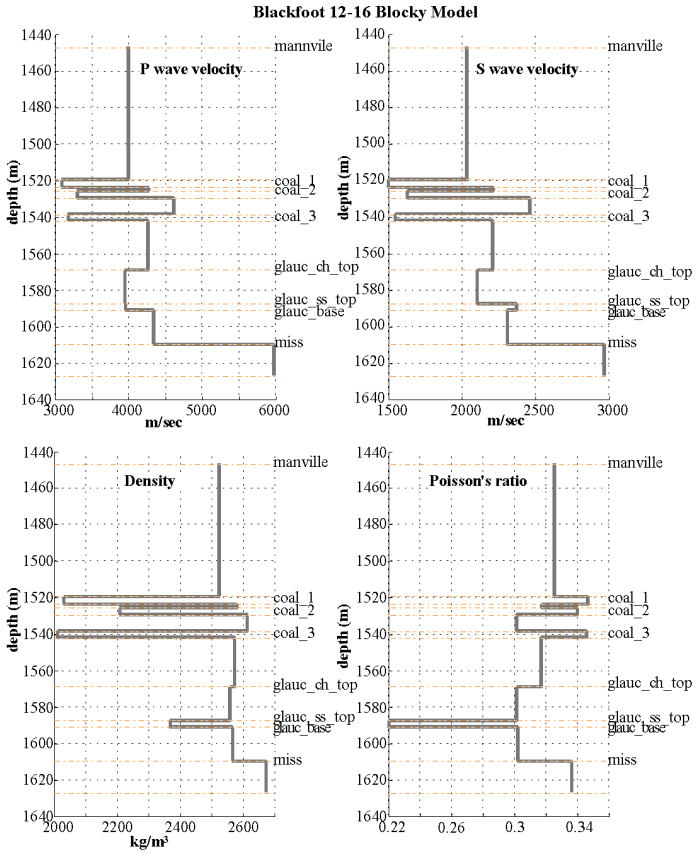

Figure 4: Blocked p-wave, s-wave, density and Poisson's ratio logs for the 12-16 well (after Simin et al.,1996). Notice the small Poisson's ratio drop (Vp/Vs decrease) at the top of the upper glauconitic channel (glauc_ch_top marker) likely due to a change in lithology or pore fluid content compared with the 08-08 well. A much larger Poisson's ratio drop can be observed at the top of the thin lower channel interval.

Contents

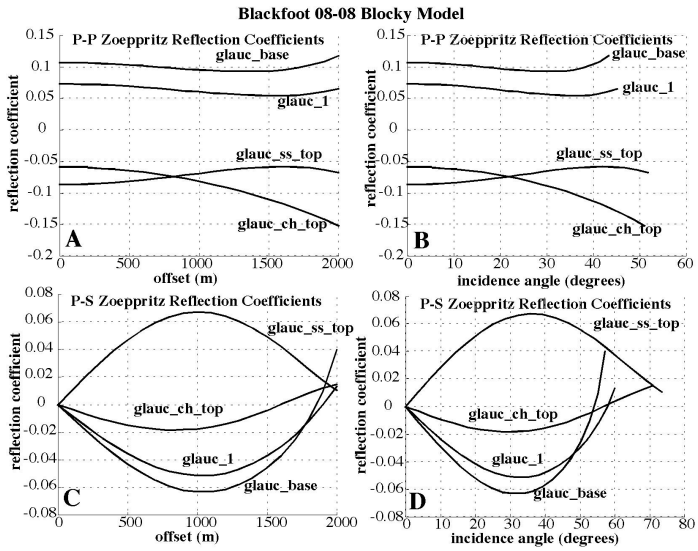

Figure 5: Reflection coefficient amplitude vs. incidence angle (or offset) at the Glauconitic interval (after Simin et al.,1996). Notice the strong P-P AVO anomaly at the top of the upper channel. A strong P-S AVO anomaly exists at the top of the lower channel.

P-WAVE WEIGHTED STACKING RESULTS

As mentioned previously, this implementation of the Smith and Gidlow method uses limited-offset migrated volumes for weighted stacking instead of applying a single weight per offset. This method was selected primary because it eliminates the need for a pre-stack migration and can be performed with less computational expense. The weights used in this method are laterally constant, and vary with depth and offset. In this implementation, we weight, then stack 5 timeslices resulting in a single timeslice representing either $\Delta\alpha/\alpha$ or $\Delta\beta/\beta$ estimates. Table 2 below shows a sample of the weights (at the top of the upper channel) applied to each timeslice prior to final stacking:

	Offset range (m)				
parameter	near	mid-near	mid	mid-far	far
$\Delta\alpha/\alpha$	0.85	0.68	0.39	0.05	-0.34
$\Delta\beta/\beta$	1.49	0.94	0.025	-1.089	-2.39
$\Delta\sigma/\sigma$	-0.64	-0.26	0.37	1.11	2.05
Δf	-.081	0.093	0.023	0.73	1.15

Table 2: Sample weights applied to the $\Delta\alpha/\alpha$, $\Delta\sigma/\sigma$ $\Delta\beta/\beta$ and Δf parameters at each offset at the top of the upper channel interval.

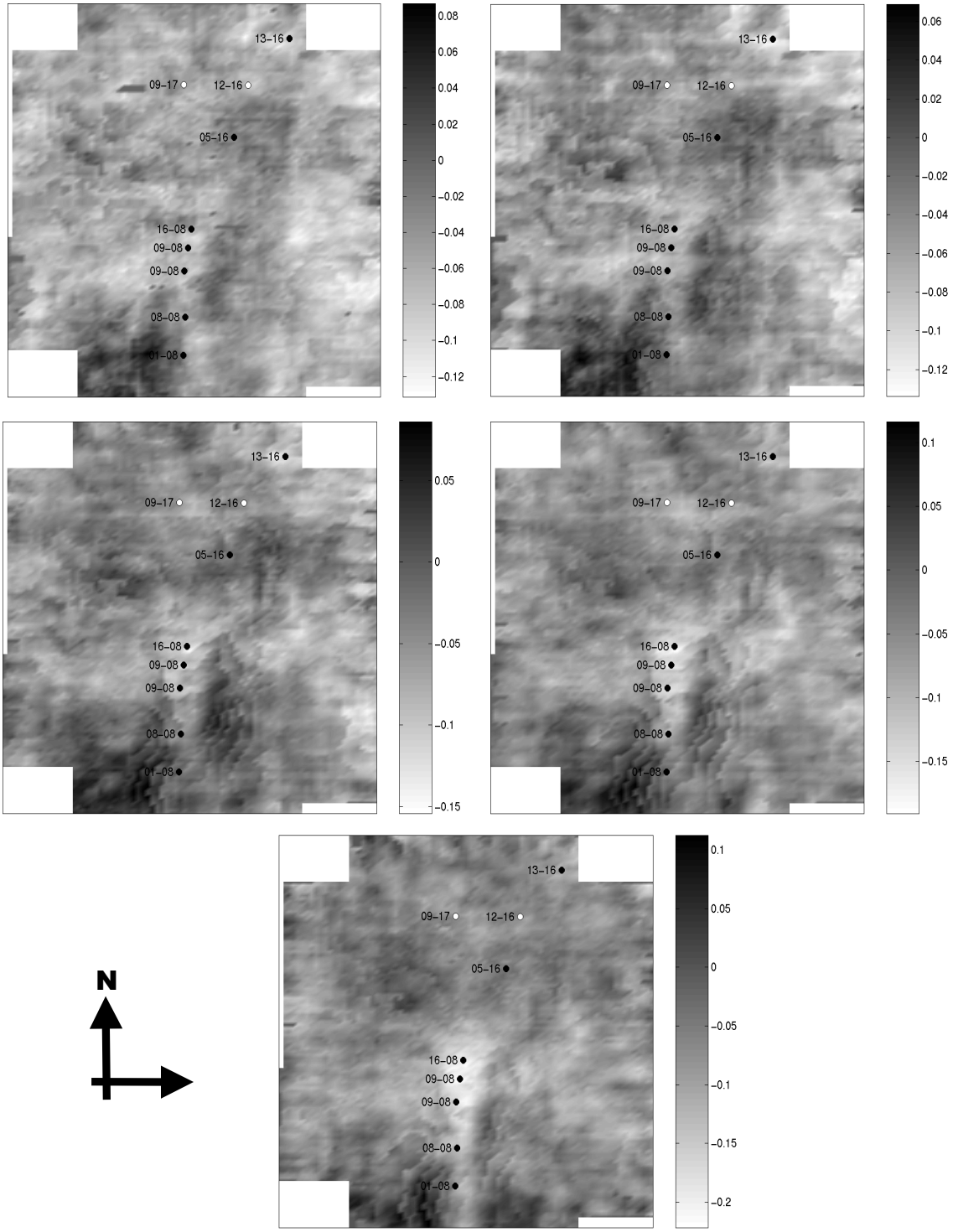

Figure 6: Near (upper left), mid-near (upper right), mid (center left), mid-far (centre right) and far (bottom) offset P-P reflectivity timeslices at the approximate top of the upper channel (12ms below the flattened lower Mannville pick). Producing wells are indicated by solid dots, regional wells and dry holes are indicated by white dots. Notice the strong negative reflectivity anomaly corresponding to the upper channel. This anomaly increases in magnitude at far offsets as predicted by the P-P reflectivity curves in figure 5.

Weighted stack displays are shown for time slices corresponding to 12ms (top of upper channel), 24ms (top of lower channel) and 32ms (base of lower channel) below the flattened lower Mannville marker (as shown in figures 7 to 9 respectively). As predicted by the reflectivity curves in figure 5, the strongest P-wave AVO anomaly occurs at the top of the upper channel. Producing wells from the Glauconitic channel interval are labeled with black well symbols, non-producing or regional wells are shown with white symbols. Producing wells may be producing from the upper, lower or both channel intervals.

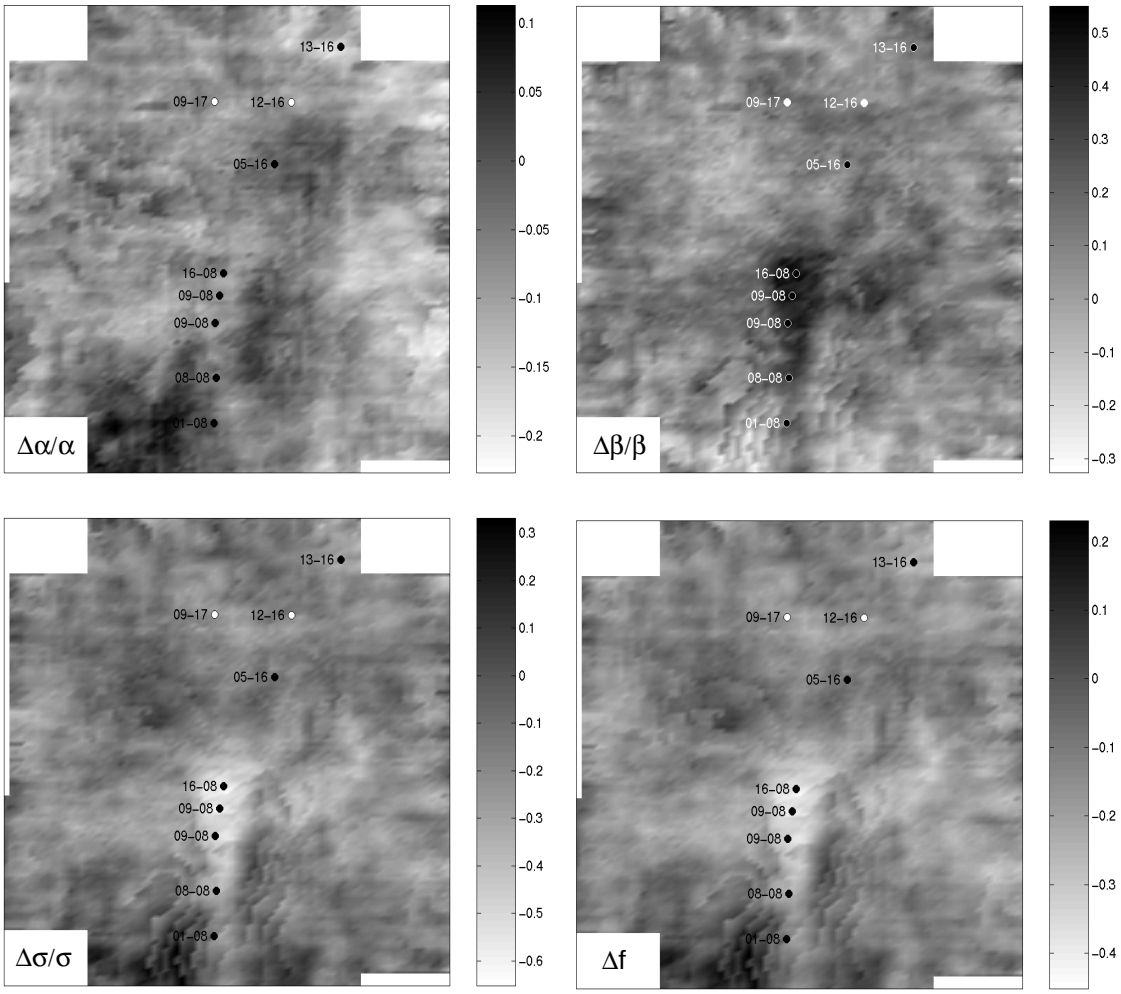

Figure 7: Weighted stack displays of $\Delta\alpha/\alpha$ (upper left), $\Delta\beta/\beta$ (upper right), $\Delta\sigma/\sigma$ (lower left) and Δf (lower right) at the top of the upper channel interval using P-P data only. The large P-wave velocity decrease predicted from well 8-8 is not readily apparent. The strong S-wave velocity increase is apparent and corresponds to the producing well trend. The estimates of the pseudo-Poisson's ratio and the fluid factor correspond closely to the channel zone.

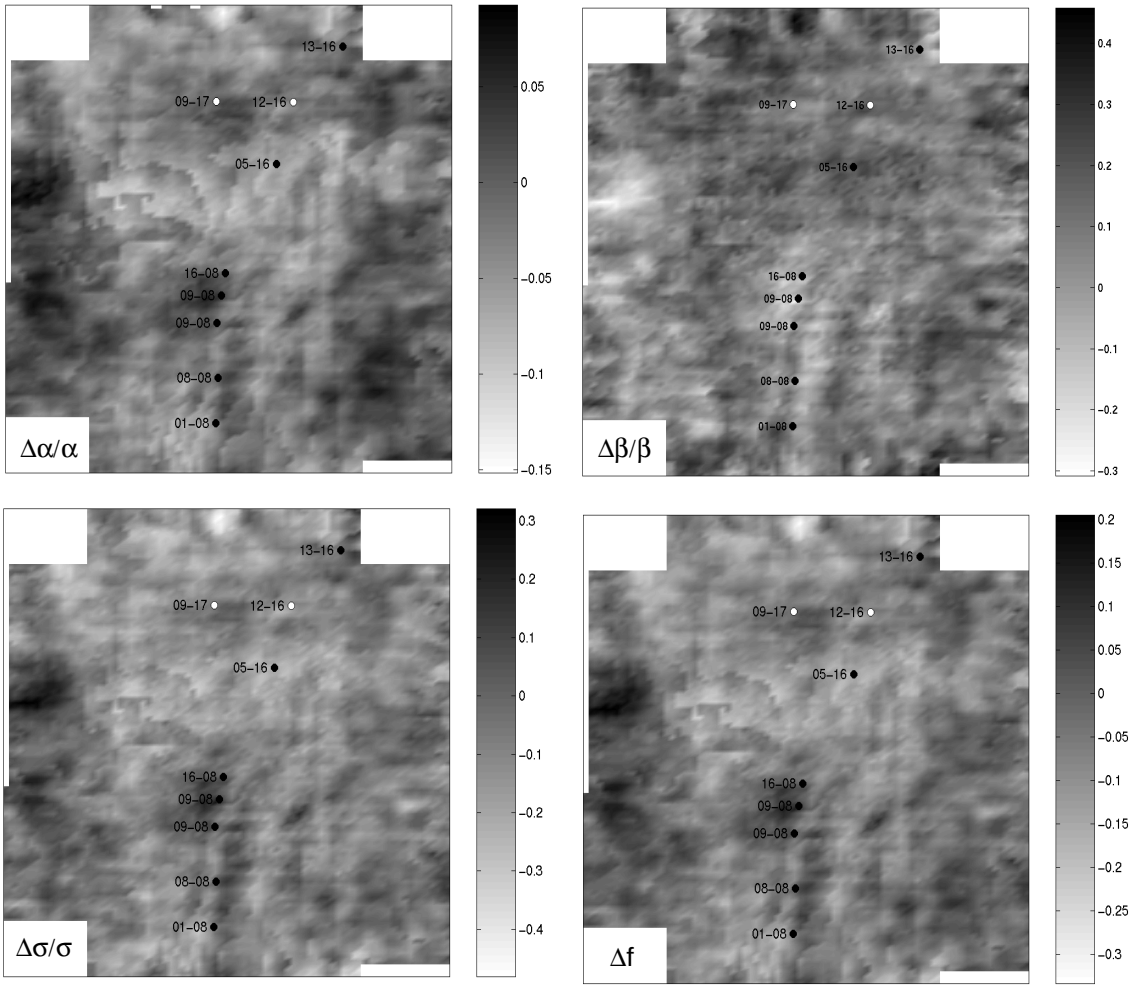

Figure 8: P-P weighted stack displays of $\Delta\alpha/\alpha$, $\Delta\beta/\beta$, $\Delta\sigma/\sigma$ and Δf at approximately the top of the lithic or lower channel interval. Notice there appears to be little indication of an anomaly in the $\Delta\alpha/\alpha$ stack. More significant anomalies appear in the $\Delta\beta/\beta$, $\Delta\sigma/\sigma$ and Δf stacks.

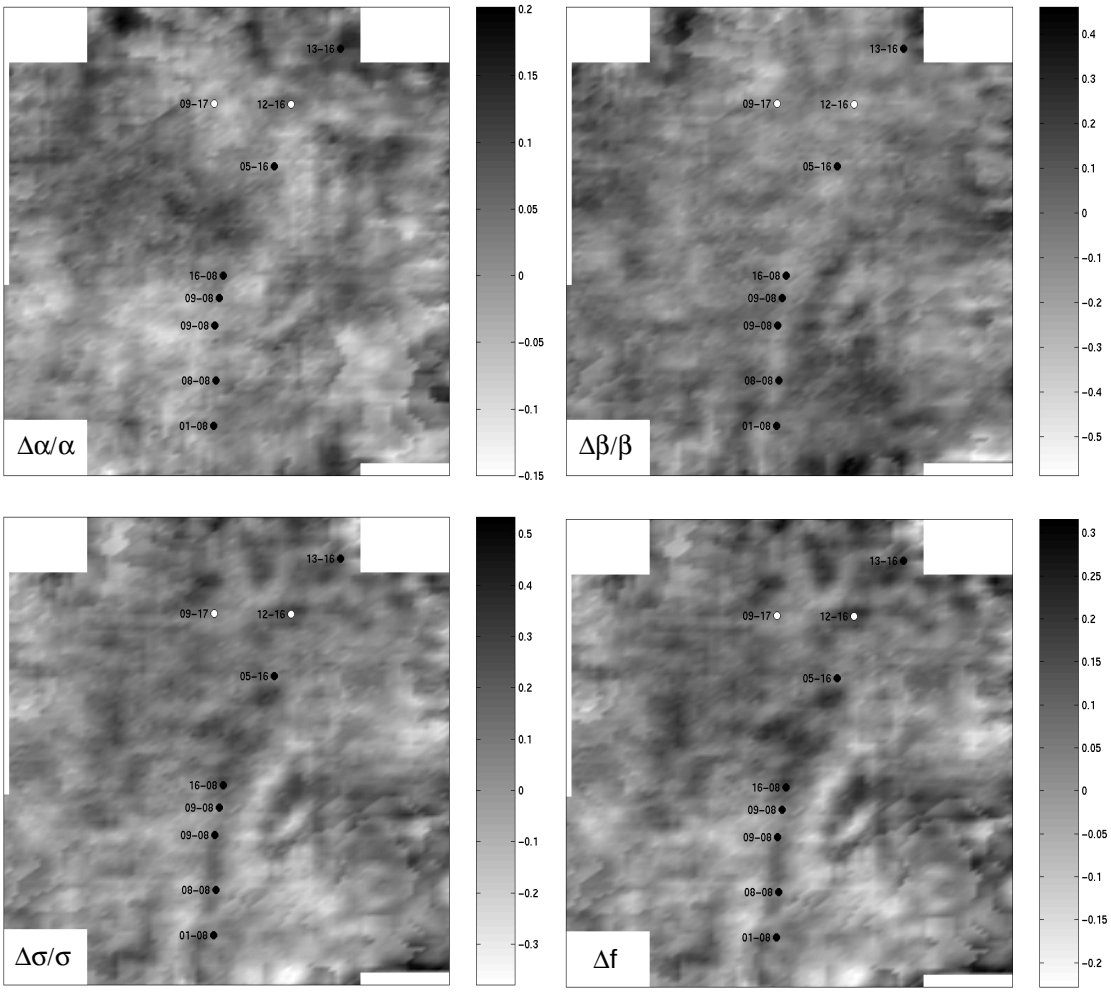

Figure 9: Weighted stack displays of and Δf at approximately the base of the lower channel. There appears to be an increase in the fluid factor reflectivity time slice in the channel zone possibly corresponding to the top of the Mississippian unconformity.

STEWART'S SIMULTANEOUS P-P AND P-S WEIGHTED STACKING RESULTS

Following event correlation and reflectivity scaling of both the vertical and radial channel datasets, this method was implemented by calculating a new set of weights for each offset range in both datasets. In all cases, this method provided a similar or better result than the Smith and Gidlow method. The channel trend appears better spatially defined, especially in the $\Delta\alpha/\alpha$ stack, and there appears to be less noise throughout each time slice. Expected anomalies along the edge of the survey, such as at the 13-16 well appear better defined, possibly due to the higher P-S fold at the edge of the survey area. The general improvement in signal-to-noise can most likely be attributed to the larger amount of data giving each parameter estimate. Generally, the P-P stack contributes more to each parameter estimate due to its larger reflection coefficient amplitude. A sample of the weights applied to each parameter at the top of the upper channel are summarized in table 3. A sample calculation of $\Delta\alpha/\alpha$ and $\Delta\beta/\beta$ at the upper channel top at the 08-08 well location is given in table 4.

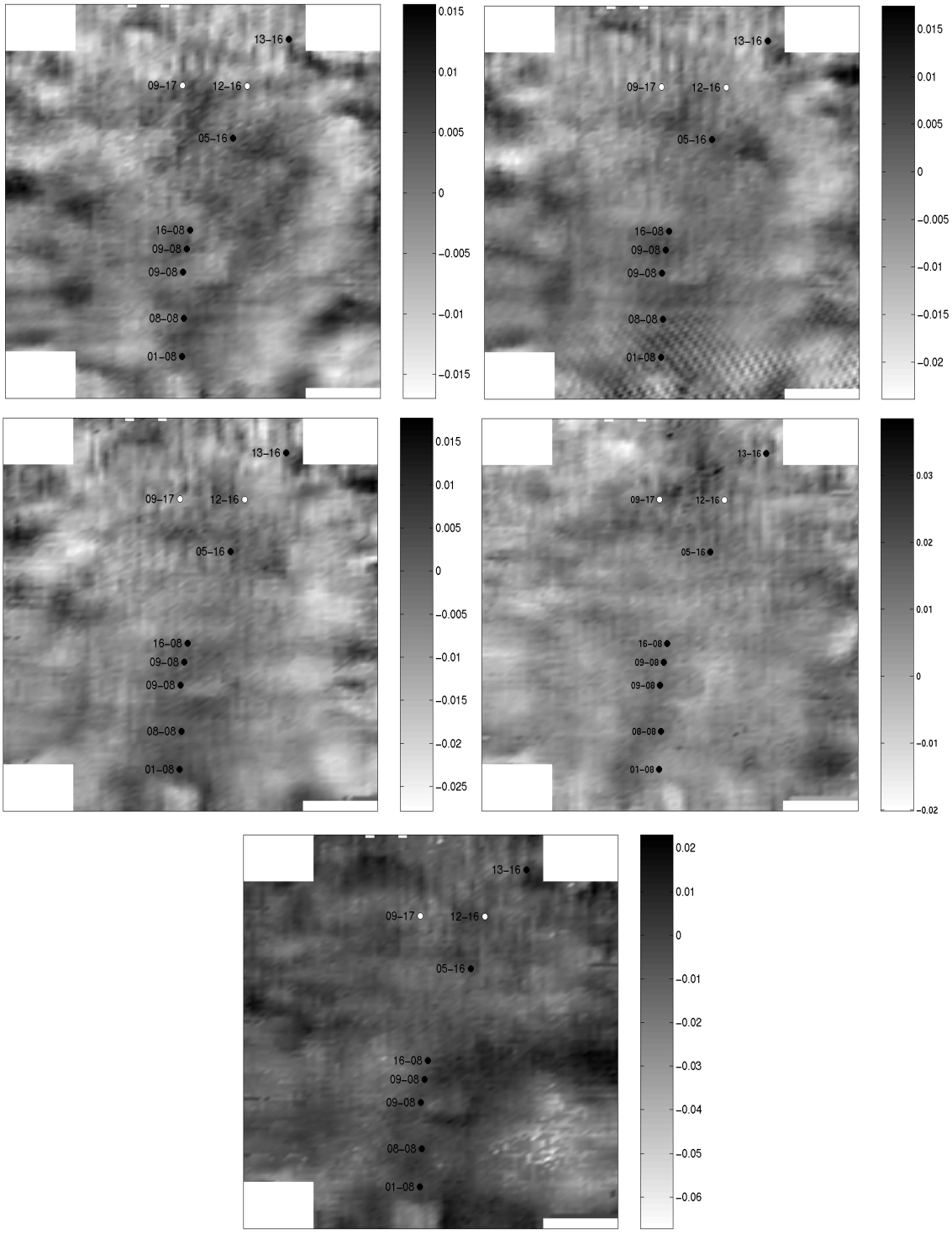

Figure 10: Near, mid-near, mid, mid-far and far offset P-S reflectivity timeslices for the radial channel dataset corresponding to the top of the upper channel (approximately 18ms below the lower Mannville marker). Events are not as apparent as the vertical channel dataset (figure 6) likely due to the decreased bandwidth and different reflectivity character with offset behavior.

Contents

parameter	offset range	$\Delta\alpha/\alpha$	$\Delta\beta/\beta$	$\Delta\sigma/\sigma$	Δf
P-P	near	0.21	-0.12	0.33	0.29
	mid-near	0.23	-0.14	0.37	0.31
	mid	0.25	-0.17	0.42	0.36
	mid-far	0.29	-0.21	0.50	0.42
	far	0.33	-0.27	0.60	0.50
P-S	near	-0.037	0.10	-0.14	-0.10
	mid-near	-0.061	0.17	-0.23	-0.17
	mid	-0.089	0.28	-0.37	-0.26
	mid-far	-0.075	0.28	-0.36	-0.25
	far	-0.021	0.22	-0.24	-0.16

Table 3: Sample weights applied for each fractional parameter at each offset range for the P-P and P-S offset gathers.

	offset	weights (for $\Delta\alpha/\alpha$ - from model)	weights (for $\Delta\beta/\beta$ - from model)	reflection coefficient (figure 5)	$\Delta\alpha/\alpha$	$\Delta\beta/\beta$	
P-P	near	0.85	1.49	-0.06	-0.092	0.15	Smith & Gidlow method
	mid-near	0.68	0.94	-0.06			
	mid	0.39	0.025	-0.07			
	mid-far	0.05	-1.08	-0.08			
	far	-0.34	-2.39	-0.09			
P-P	near	0.21	-0.12	-0.06	-0.093	0.060	Stewart's simultaneous inversion method
	mid-near	0.23	-0.14	-0.06			
	mid	0.25	-0.17	-0.07			
	mid-far	0.29	-0.21	-0.08			
	far	0.33	-0.27	-0.09			
P-S	near	-0.037	0.10	-0.01			
	mid-near	-0.061	0.17	-0.018			
	mid	-0.089	0.28	-0.019			
	mid-far	-0.075	0.28	-0.008			
	far	-0.021	0.22	0.008			

Table 4: Sample calculation of $\Delta\alpha/\alpha$ and $\Delta\beta/\beta$ weighted stacks at the top of the Glauconitic channel at the 08-08 well location. $\Delta\alpha/\alpha$ and $\Delta\beta/\beta$ are calculated by multiplying each weight by its associated reflection coefficient and taking the sum of the result. Notice both $\Delta\alpha/\alpha$ estimates closely correspond to the $\Delta\alpha/\alpha$ result calculated from the P-wave velocity log in figure 4 ($\Delta\alpha/\alpha$ of approximately -0.10). The $\Delta\beta/\beta$ results are both quite different and should correspond to a $\Delta\beta/\beta$ of 0.08 from figure 4.

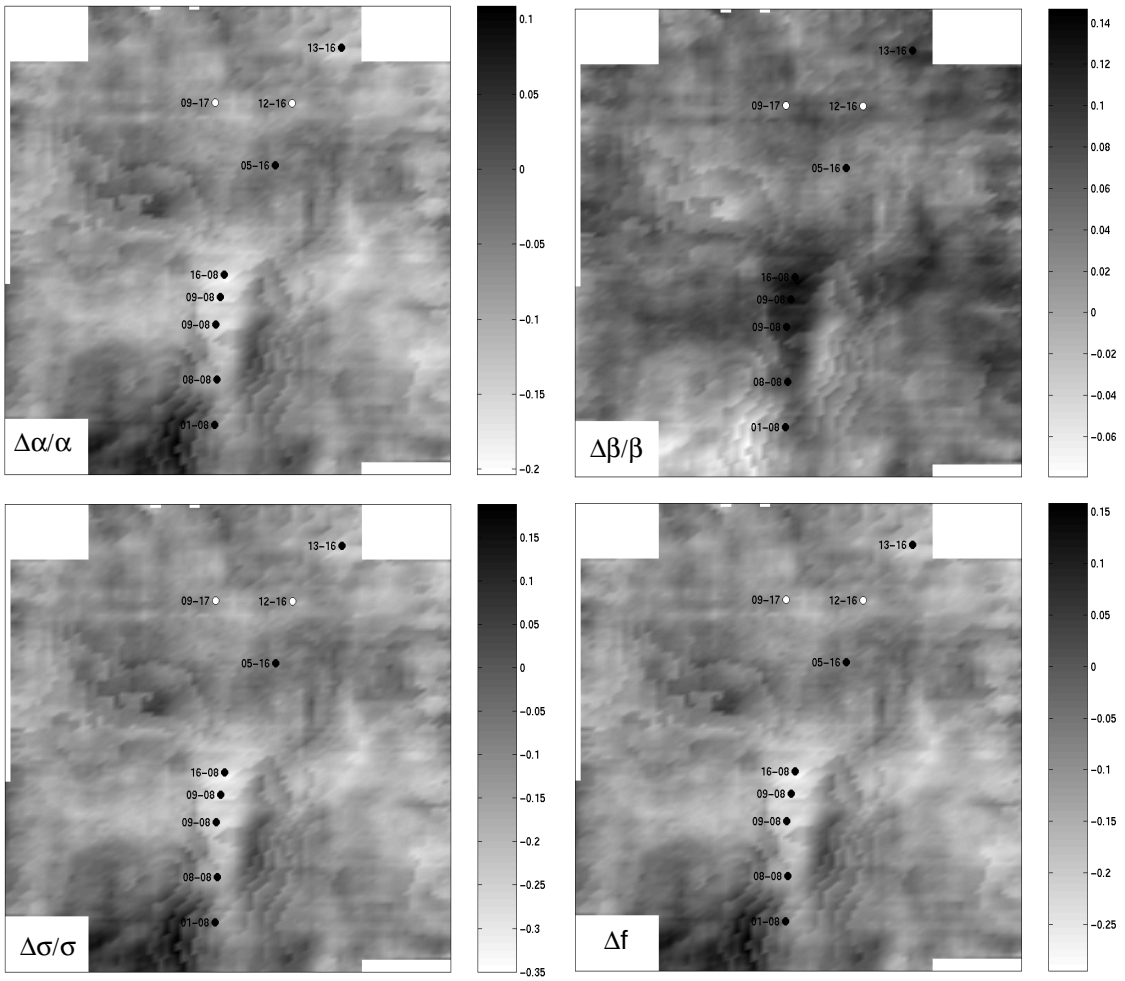

Figure 11: Weighted stack displays of at the top of the upper channel interval using both P-P and P-S seismic data. Note the improvement on the estimate of $\Delta\alpha/\alpha$ compared with figure 7. Also note the more apparent velocity anomaly at the 13-16 well compared with figure 7.

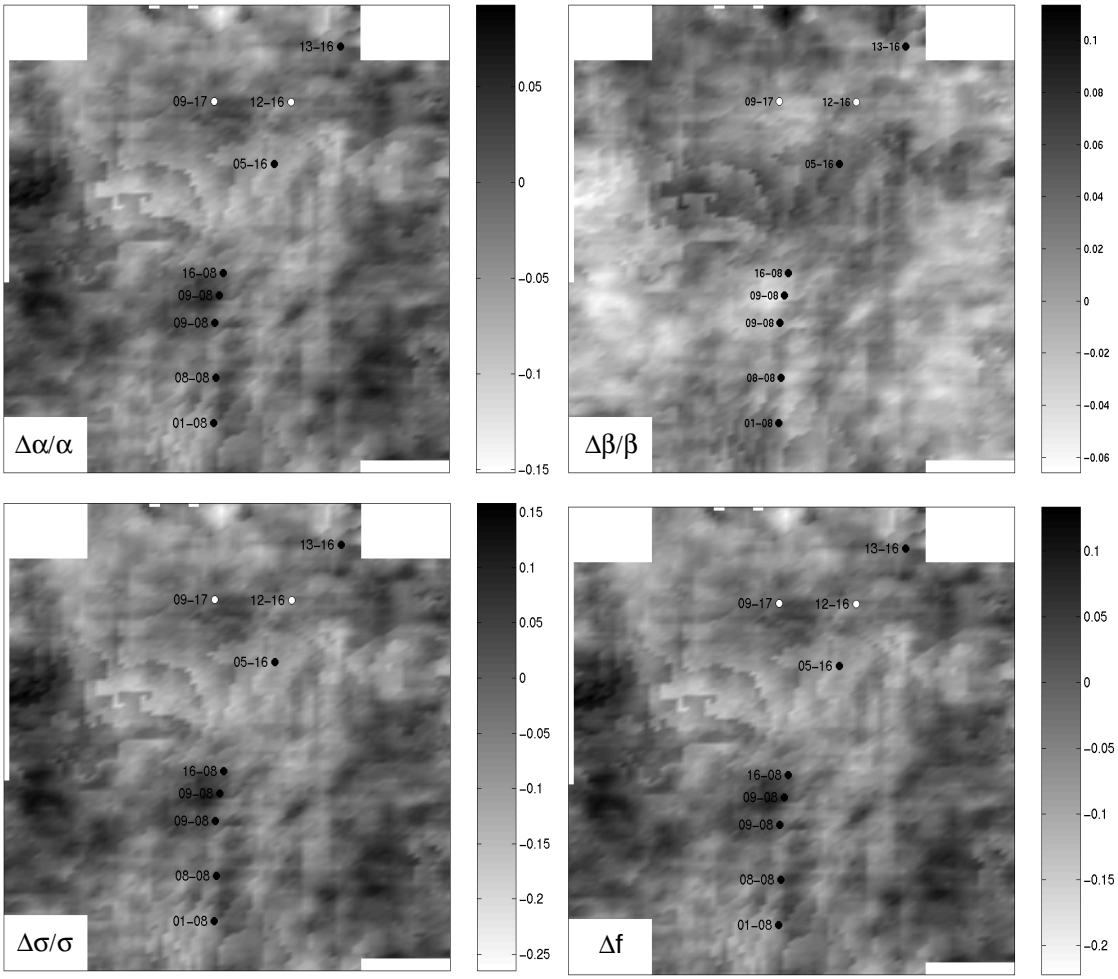

Figure 12: Weighted stack displays of $\Delta\alpha/\alpha$, $\Delta\beta/\beta$, $\Delta\sigma/\sigma$ and Δf at the top of the lithic or lower channel interval using both P-P and P-S data. Notice the channel anomaly appears more distinct in the $\Delta\alpha/\alpha$ stack compared with figure 8. The other $\Delta\beta/\beta$, $\Delta\sigma/\sigma$ and Δf stacks appear little changed except for a slight improvement in contrast.

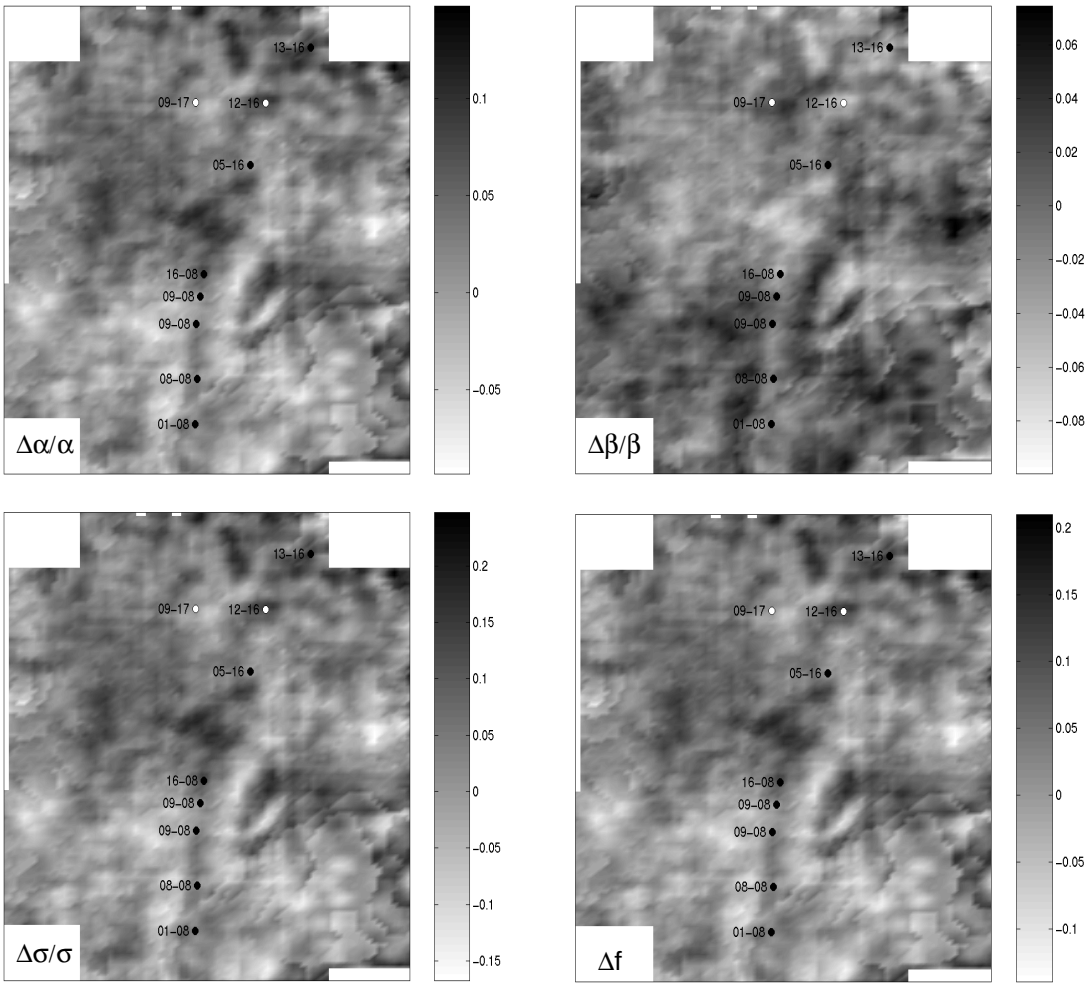

Figure 13: Weighted stack displays of $\Delta\alpha/\alpha$, $\Delta\beta/\beta$, $\Delta\sigma/\sigma$ and Δf using both P-P and P-S seismic data at approximately the base of the lower channel. Notice the greater definition of the channel zone in the $\Delta\alpha/\alpha$ and $\Delta\beta/\beta$ stacks compared with figure 9. Again there appears to be greater contrast between the channel feature and other regional features.

CONCLUSIONS

A simultaneous P-P and P-S weighted stacking inversion method has been implemented and compared to the Smith and Gidlow method utilizing only P-P seismic data. Initial results show there is a general improvement using both types of data, events appear more coherent and signal-to-noise appears to have increased.

FUTURE WORK

We plan to develop a similar method to estimate Lame parameters using this simultaneous P-P and P-S inversion method. We also plan to develop other inversion methods using multi-component seismic data.

ACKNOWLEGDEMENTS

We wish to thank the sponsors of the Blackfoot 3C-3D group shoot and all the sponsors of the CREWES Project.

REFERENCES

Aki, K., and Richards, P.G., 1980, Quantitative seismology: Theory and methods, Vol. 1: W.H. Freeman and Co.

Castagna, J.P, Batzle, M.L., and Kan, T.K., 1993, Rock physics: the link between rocks properties and AVO response in Castagna, J.P., and Backus, M.M., Eds., Offset-dependant reflectivity – Theory and practice of AVO analysis, Soc. Expl. Geophys., 135-171.

Danbom, S.H., and Domenico, S.N., 1986, Shear-wave exploration: Geophysical Development Series, Volume 1, Soc. Expl. Geophys.

Fatti, J.L., Smith, G.C., Vail, P.J., Strauss, P.J. and Levitt, P.R., 1994, Detection of gas in sandstone reservoirs using AVO analysis: A 3-D seismic case history using the Geostack technique: Geophysics, 59, 1362-1376.

Gardner, G.H.F., Gardner, L.W., and Gregory, A.R., 1974, Formation velocity and density, the diagnostic basics for stratigraphic traps: Geophysics, 39, 770-780.

Garotta, R., and Granger, P.Y., 1987, Comparison of responses of compressional and converted waves on a gas sand: 57th Ann. Internat. Mtg., Soc. Expl. Geophys., Expanded Abstracts, 627-630.

Goodway, B., Chen, T., and Downton, J., 1997, Improved AVO fluid detection and lithology discrimination using Lame petrophysical parameters: "λρ", "μρ", and "λ/μ fluid stack", from P and S inversions: 67th Ann. Internat. Mtg., Soc. Expl. Geophys., Expanded Abstracts.

Koefoed, O., 1955, On the effect of Poisson's ratio of rock strata on the reflection coefficients of plane waves, Geophysical Prospecting 3, 381-387.

Lu, H., and Margrave, G.F., 1998, Reprocessing of the Blackfoot 3C-3D dataset: The CREWES Research Report, Vol. 10, ch.31.

Margrave, G.F. and Foltinek, D.S., 1995, Sythetic P-P and P-SV cross sections: CREWES Annual Research Report, Vol. 7.

Miles, D.R., and Gassaway, G.S., 1989, Three-component AVO analysis: 59th Ann. Internat. Mtg., Soc. Expl. Geophys., Expanded Abstracts, 706-708.

Miller, S.M., Aydemir, E.O., and Margrave, G.F., 1995, Preliminary interpretation of P-P and P-S seismic data from the Blackfoot broad-band survey: CREWES Annual Research Report, Chapter 42.

Rutherford, S.R. and Williams, R.H., 1989, Amplitude-versus-offset variations in gas sands: Geophysics, 54, no. 6. 680-688.

Shuey, R.T., 1985, A simplification of the Zoeppritz equations, Geophysics 50, 609-614.

Simin, V., Harrison, M.P., and Lorentz, G.A., 1996, Processing the Blackfoot 3C-3D survey: The CREWES Research Report, Vol. 8, ch. 39.

Simin, V., Margrave, G.F. and Yang, G.C., 1996, AVO measurements for P-P and P-S data in the Blackfoot 3C-3D dataset: The CREWES Research Report, Vol. 8, ch. 42.

Smith, G.C., and Gidlow, P.M., 1987, Weighted stacking for rock property estimation and detection of gas: Geophysical Prospecting 35, 993-1014.

Stewart, R.R., 1990, Joint P and P-SV Inversion: The CREWES Research Report, Vol. 3, 112-115.

Swan, H.W., 1993¸ Properties of Direct AVO Hydrocarbon Indicators in Castagna, J.P., and Backus, M.M., Eds., Offset-dependant reflectivity – Theory and practice of AVO analysis, Soc. Expl. Geophys., 78-92.

Vestrum, R.W., and Stewart, R.R., 1993, Joint P and P-SV inversion: Application and testing: The CREWES Research Report, Vol. 5, ch. 13.